

Title No. 111-S36

# Flexural Capacity of Fiber-Reinforced Polymer Strengthened Unbonded Post-Tensioned Members

by Fatima El Meski and Mohamed Harajli

Experimental and analytical investigations were carried out for evaluating the nominal moment capacity of unbonded post-tensioned members when strengthened using external fiber-reinforced polymer (FRP) composites. In the experimental part of the study, 36 simply supported specimens were tested to failure. The main test parameters included area of internal tension reinforcement, area of external FRP reinforcement, span-depth ratio of the member, profile of the prestressing tendons, and type of concrete structural system. In the analytical part of the study, a design-oriented procedure for evaluating the nominal moment capacity of FRP-strengthened post-tensioned members with internal or external unbonded tendon systems is developed. The procedure is consistent with the approach proposed in ACI Committee 440 report for reinforced concrete or bonded prestressed concrete members, and is applicable for both simply supported and continuous members. The accuracy of the design approach was verified by comparing it with the test results of the experimental part of this investigation.

**Keywords:** fiber-reinforced polymer; flexure; prestressing; post-tensioning; strengthening; unbonded tendons.

## INTRODUCTION AND BACKGROUND LITERATURE

The flexural capacity of bonded prestressed concrete members can be evaluated in accordance with the general ACI Building Code<sup>1</sup> approach and the guidelines recommended by ACI Committee 440<sup>2</sup> by accounting for the effect of fiber-reinforced polymer (FRP) reinforcement as follows

$$M_n = A_{ps}f_{ps}(d_p - \beta_1c/2) + A_s f_s (d - \beta_1c/2) + \psi_f A_f E_f \epsilon_f (d_f - \beta_1c/2) \quad (1)$$

where

$$f_{ps} = F(\epsilon_{ps}) \quad (2)$$

$$f_s = E_s \epsilon_s \leq f_y \quad (3)$$

$$\epsilon_{ps} = \epsilon_{pe} + \epsilon_{ce} + \epsilon_{cu} \left( \frac{d_p - c}{c} \right) \quad (4)$$

$$\epsilon_{ce} = \frac{1}{E_c} \left( \frac{A_{ps} f_{se}}{A_c} + \frac{A_{ps} f_{se} e^2}{I_g} \right) \quad (5)$$

$$\epsilon_s = \epsilon_{cu} \left( \frac{d - c}{c} \right) \quad (6)$$

$$\epsilon_f = \epsilon_{cu} \left( \frac{d_f - c}{c} \right) - \epsilon_{bi} \leq \epsilon_{fd} \quad (7)$$

$$\epsilon_{fd} = 0.41 \sqrt{\frac{f'_c}{n_f E_f t_f}} \leq 0.9 \epsilon_{fu} \quad (8)$$

$$c = \frac{A_{ps} f_{ps} + A_s f_s + A_f (f_f = E_f \epsilon_f)}{\alpha_1 f'_c \beta_1 b} \quad (9)$$

in which  $c$  is the neutral axis depth of the section at nominal flexural strength;  $A_{ps}$  and  $d_p$  are area and depth of the unbonded prestressing steel (PS);  $A_f$  is area and  $d_f$  is depth of the FRP reinforcement; and  $A_s$  is area of bonded ordinary reinforcing steel (RS) at the section under consideration. For slabs, the areas  $A_{ps}$ ,  $A_s$ , and  $A_f$  are per unit width  $b$  of the slab section.  $\epsilon_{ce}$  is precompression strain in concrete at the level of the prestressed tendons;  $A_c$  and  $I_g$  are area and moment of inertia of the gross section, respectively;  $e$  is eccentricity of the tendons;  $E_c$ ,  $E_s$ , and  $E_f$  are modulus of elasticity of concrete, steel, and FRP reinforcement, respectively;  $\epsilon_f$  and  $f_f$  are strain and stress in the FRP reinforcement, respectively;  $\epsilon_{fu}$  is rupture strain of the FRP reinforcement;  $F$  is the material stress-strain relationship of the prestressing reinforcement;  $\epsilon_{pe}$ ,  $f_{se}$ ,  $\epsilon_{ps}$ , and  $f_{ps}$  are effective strain, effective stress, strain, and stress at ultimate, respectively, in the prestressing steel ( $\epsilon_{pe} = f_{se}/E_{ps}$ , where  $E_{ps}$  is the modulus of elasticity of the prestressing steel);  $\epsilon_s$ ,  $f_s$ , and  $f_y$  are strain, stress, and yield stress, respectively, for the ordinary RS;  $f'_c$  is concrete cylindrical compressive strength;  $\epsilon_{cu}$  is usable concrete strain at compression failure (equal to 0.003 in accordance with ACI 318-11<sup>1</sup>);  $\alpha_1 = 0.85$  corresponding to a concrete strain in the outermost compression fiber equal to  $\epsilon_{cu}$ ;  $\beta_1$  is concrete strength factor defined in section 10.2.7.3 of the ACI Building Code<sup>1</sup>;  $\epsilon_{bi}$  is initial substrate strain at which the FRP was applied for strengthening (ACI Committee

ACI Structural Journal, Vol. 111, No. 2, March-April 2014.

MS No. S-2012-168.R2, doi:10.14359/51686565, was received January 10, 2013, and reviewed under Institute publication policies. Copyright © 2014, American Concrete Institute. All rights reserved, including the making of copies unless permission is obtained from the copyright proprietors. Pertinent discussion including author's closure, if any, will be published ten months from this journal's date if the discussion is received within four months of the paper's print publication.

440<sup>2</sup>), determined using elastic cracked section analysis, considering all loads that will be on the member during the FRP installation;  $\epsilon_{fd}$  is strain in the FRP reinforcement at which FRP debonding failure occurs;  $n_f$  and  $t_f$  are number of FRP layers and thickness per one layer, respectively; and  $\psi_f$  is the FRP strength-reduction factor recommended by ACI Committee 440,<sup>2</sup> which is taken equal to 0.85 for flexure.

To calculate the nominal moment capacity of FRP-strengthened reinforced concrete (RC) or bonded PC members, ACI Committee 440<sup>2</sup> recommends using a trial-and-error procedure for estimating the neutral axis depth  $c$  until the requirements of strain compatibility and force equilibrium across the depth of the critical section are satisfied (Eq. (9)). Also, two modes of flexural failure are recognized by ACI Committee 440: 1) concrete crushing—that is, when the strain in the outermost concrete compression fiber reaches  $\epsilon_{cu}$  before FRP failure; and 2) FRP failure before concrete crushing. FRP failure could occur either by FRP rupture, cover delamination, or FRP debonding. Accordingly, ACI Committee 440<sup>2</sup> limits, conservatively, the strain in the FRP reinforcement at which FRP failure takes place to the debonding strain  $\epsilon_{fd}$  (Eq. (8)). When the strain in the FRP reaches its limiting strain  $\epsilon_{fd}$  before the concrete compression strain reaches  $\epsilon_{cu}$ , the concrete compression strain  $\epsilon_{cu}$  in Eq. (2) through (9) should be replaced by its actual value expressed as a function of  $\epsilon_{fd}$  as follows

$$\epsilon_c = (\epsilon_{fd} + \epsilon_{bi}) \left( \frac{c}{d_f - c} \right) \quad (10)$$

The values of  $\alpha_1$  and  $\beta_1$ , which are now different from their values when  $\epsilon_c = \epsilon_{cu}$ , can be estimated with reasonable accuracy using the following expressions recommended by ACI Committee 440,<sup>2</sup> which were derived assuming a parabolic relationship for the stress-strain curve of concrete in compression

$$\beta_1 = \frac{4\epsilon'_c - \epsilon_c}{6\epsilon'_c - 2\epsilon_c} \quad (11)$$

$$\alpha_1 = \frac{3\epsilon'_c \epsilon_c - (\epsilon_c)^2}{3\beta_1 (\epsilon'_c)^2} \quad (12)$$

where  $\epsilon'_c$  is the strain corresponding to  $f'_c$ , which can either be taken equal to 0.002 or calculated more accurately as  $\epsilon'_c = 1.7f'_c/E_c$ .

### RESEARCH SIGNIFICANCE

An experimental study was carried out and a design-oriented approach was developed for evaluating the nominal flexural capacity  $M_n$  of unbonded PC members when strengthened using external FRP composites. The design approach builds on a previous model generated for evaluating the stress in unbonded tendons at ultimate in simply supported or continuous members, and is consistent with the

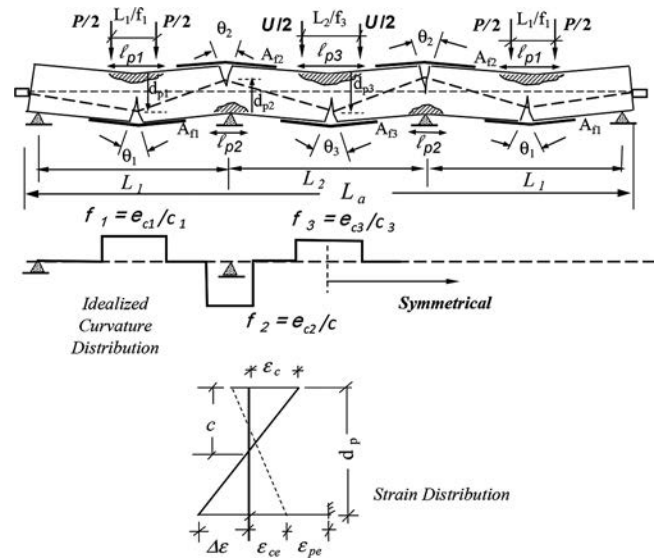


Fig. 1— FRP-strengthened continuous unbonded member with multi-collapse mechanisms.

ACI Committee 440<sup>2</sup> guidelines for calculating  $M_n$  for FRP strengthened bonded PC or RC members. The approach is validated for simply supported members by comparing with the test results generated in the experimental part of this investigation.

### STRESS IN UNBONDED TENDONS AT ULTIMATE

While the approach recommended by ACI Committee 440<sup>2</sup> for estimating  $M_n$  for FRP strengthened RC or bonded PC members is simple because it relies on commonly adopted and familiar principles, it is not as straightforward for PC members with unbonded tendons. In PC members with internal or external unbonded tendons, because the unbonded steel slips relative to the surrounding concrete, the strain or stress  $f_{ps}$  in the prestressing steel that develops at nominal flexural strength relies on the deformation of the member as a whole. This makes the evaluation of the corresponding strain and stress member, rather than section, dependent.

Several design approaches are available for predicting the stress in unbonded tendons at ultimate.<sup>1,3,4</sup> A comparative evaluation of these approaches has been discussed in detail elsewhere.<sup>5</sup> Using plastic analysis and the concept of collapse mechanism in continuous members, as well as idealization of the curvature distribution along the span lengths at nominal flexural strength as shown in Fig. 1 (for  $\epsilon_c = \epsilon_{cu}$ , and  $A_f = 0.0$ ) and further incorporating an empirically derived expression for the equivalent plastic hinge length for unbonded members given as<sup>5</sup>  $l_p = (20.7/f + 10.5)c$ , Harajli<sup>6</sup> developed the following general and yet elegant expression for calculating the strain  $\epsilon_{ps}$  in unbonded tendons at ultimate

$$\epsilon_{ps} = \epsilon_{pe} + \phi_{ps} \left( N_p \epsilon_{cu} \frac{d_p}{L_a} - N_p (\epsilon_{cu} - \epsilon_{ce}) \frac{c}{L_a} \right) \quad (13)$$

where

$$N_p = \left( \frac{20.7}{f} + 10.5 \right) n_p^+ + 10.5 n_p^- \quad (14)$$

in which  $c$  is the neutral axis depth at the section under consideration;  $\epsilon_{ce}$  is calculated using Eq. (5) by neglecting the effect of the secondary moment due to prestressing in continuous members;  $L_a$  is the total length of tendons between anchorages;  $N_p$  (Eq. (14)) is a parameter that combines the effect of member continuity and type of applied load;  $f = \infty$  for a single concentrated load, 3.0 for two-third point loads, and 6.0 for uniform load application, respectively;  $n_p^+$ ,  $n_p^-$  are the number of positive and negative plastic hinges, respectively, that develop in the process of forming a collapse mechanism; and  $\phi_{ps}$  is a stress-reduction factor taken equal to 0.7. Note that because the live load in buildings and bridges is seldom a concentrated load, and also because the dead load is uniformly distributed, the multiplier  $(20.7/f + 10.5)$  of the positive number of plastic hinge(s)  $n_p^+$  can always be set equal to 14.0 to correspond to uniform load application.<sup>6</sup>

Equations (13) and (14) were developed with the perspective that the calculation of the stress in unbonded tendons at ultimate in continuous members differs from one critical section to another. That is, the stress at a critical section depends on the pattern of applied load and the consequent collapse mechanism that would potentially develop for producing the maximum factored design moment at that section. For the hypothetical case of Fig. 1, in which collapse mechanisms are assumed to form in all spans:  $n_{p1}^+ = 2.0$ ,  $n_{p2}^- = 2.0$ , and  $n_{p3}^+ = 2.0$ . In actual design, however, the numbers of plastic hinges  $n_p^+$  and  $n_p^-$  are obtained from the collapse mechanisms that develop when loading the minimum number of spans for producing maximum moment at the section under consideration. For instance, in simply supported members, one span is loaded, and hence  $n_p^+ = 1.0$ ,  $n_p^- = 0.0$ , and  $N_p = 14.0$ . For continuous members, collapse mechanisms (a), (b), (c), (d), and (e) in Fig. 2, and corresponding values of  $N_p$  are recommended<sup>6</sup> for computing the tendon stress  $f_{ps}$  and the nominal moment capacity at the maximum positive moment section in exterior spans; negative moment section at the interior support of a two-span member; maximum positive moment section in interior spans; negative moment section at the first interior support; and negative moment section at the remaining interior supports of members with more than two spans, respectively.

### PROPOSED APPROACH FOR COMPUTING $M_N$ IN FRP STRENGTHENED UNBONDED MEMBERS

Using Eq. (13) but neglecting the precompression strain  $\epsilon_{ce}$  due to its minor effect on the tendon stress in unbonded members, particularly when compared with bonded members, and considering that the flexural strength may be controlled by FRP failure at which  $\epsilon_c \leq \epsilon_{cu}$  (Fig. 1), the following expression is recommended for computing the strain  $\epsilon_{ps}$  in unbonded tendons of FRP-strengthened simply

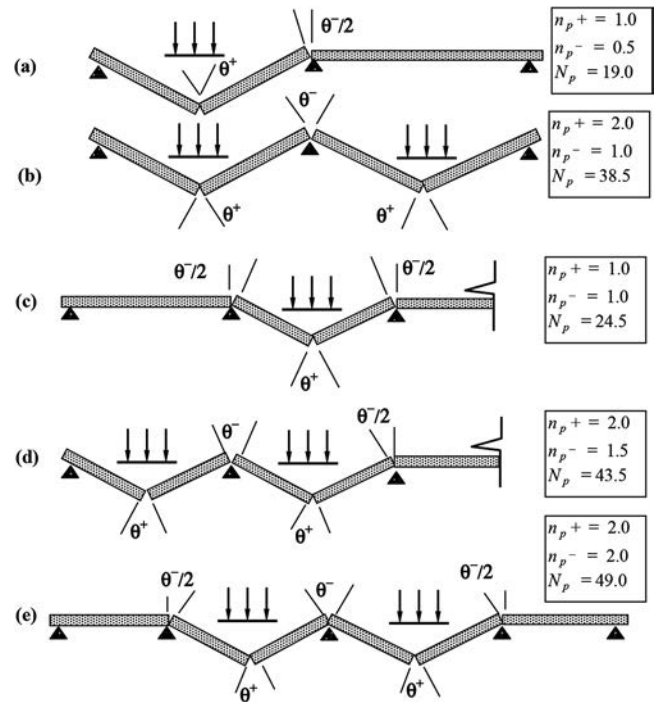


Fig. 2—Loading pattern and corresponding values of continuity parameter  $N_p$  for continuous members.

supported or continuous members at nominal flexural strength

$$\epsilon_{ps} = \epsilon_{pe} + \phi_{ps} N_p \epsilon_c \left( \frac{d_p - c}{L_a} \right) \quad (15)$$

Recognizing that the stress in the prestressing steel seldom exceeds yield and limiting the corresponding stress to  $0.95f_{py}$ <sup>6</sup> allows the use of a linear relationship between the stress and strain in the prestressing steel, that is,  $f_{ps} = E_{ps}\epsilon_{ps}$ , leading to

$$f_{ps} = f_{se} + \frac{\phi_{ps} N_p E_{ps} \epsilon_c}{L_a / d_p} \left( 1 - \frac{c}{d_p} \right) \leq 0.95 f_{py} \quad (16)$$

The force equilibrium across the depth of the critical section, assuming rectangular section or rectangular section behavior, is expressed as

$$A_{ps} f_{ps} + A_f f_s + A_f E_f \epsilon_f = \alpha_1 f'_c b \beta_1 c \quad (17)$$

It should be noted that for unbonded members without FRP reinforcement (that is,  $A_f = 0.0$  and  $\alpha_1 = 0.85$ ), the value of  $c$  from Eq. (17) can be integrated in Eq. (16) to produce a direct expression for computing  $f_{ps}$  in unbonded members at ultimate.<sup>6</sup>

Using Eq. (15), (16), and (17), the following step-by-step procedure can be adopted for evaluating the nominal moment capacity  $M_n$  of FRP strengthened unbonded post-tensioned members.

## Case I—Flexural capacity controlled by concrete crushing

*Step 1*—Assume that the nominal flexural strength at a critical section is controlled by concrete crushing—that is,  $\epsilon_f$  calculated using Eq. (7) is less than or equal to  $\epsilon_{fd}$  (Eq. (8)). This implies that  $\epsilon_c = \epsilon_{cu}$ ,  $\alpha_1 = 0.85$ , and  $\beta_1$  is as defined in section 10.2.7.3 of the ACI Building Code.<sup>1</sup> Replacing  $f_{ps}$  from Eq. (16) into Eq. (17) and assuming that the RS yields, that is,  $f_s = f_y$ , leads to the following quadratic equation for calculating the neutral axis depth at nominal flexural strength at the section under consideration

$$c = \frac{B + \sqrt{B^2 + 4AC}}{2A} \quad (18)$$

where

$$A = 0.85\beta_1 f_c' b + \frac{\phi_{ps} N_p A_{ps} E_{ps} \epsilon_{cu}}{L_a} \quad (19a)$$

$$B = A_{ps} \left( f_{se} + \frac{\phi_{ps} N_p E_{ps} \epsilon_{cu} d_p}{L_a} \right) + A_s f_y - A_f E_f (\epsilon_{cu} + \epsilon_{bi}) \quad (19b)$$

$$C = A_f E_f \epsilon_{cu} d_f \quad (19c)$$

in which  $N_p$  is as defined previously (Fig. 2). For simply supported members,  $N_p = 14.0$ .

*Step 2*—Check if  $\epsilon_f$  (Eq. (7)) is indeed  $\leq \epsilon_{fd}$ . Also check if the strain  $\epsilon_s$  in the RS is larger than the yield strain  $\epsilon_y$ . If  $\epsilon_f \leq \epsilon_{fd}$  while  $\epsilon_s$  is less than  $\epsilon_y$ , repeat Step 1 for recalculating more accurately the neutral axis depth using Eq. (18) in which the coefficients  $A$ ,  $B$ , and  $C$  are revised by substituting  $f_s = E_s \left( \epsilon_s = \epsilon_{cu} \frac{d-c}{c} \right)$  for  $f_y$  in Eq. (17).

*Step 3*—Calculate  $f_{ps}$  from Eq. (16) corresponding to  $\epsilon_c = \epsilon_{cu}$ , and  $f_s$  from Eq. (3), and hence calculate the nominal moment capacity  $M_n$  from Eq. (1).

## Case II—Flexural capacity controlled by FRP failure

*Step 4*—If  $\epsilon_f$  calculated from Step 2 is greater than  $\epsilon_{fd}$  (Eq. (8)), then FRP failure occurs before the strain  $\epsilon_c$  reaches  $\epsilon_{cu}$ . In this case, the strain  $\epsilon_f$  in the FRP reinforcement is equal to  $\epsilon_{fd}$ , and hence, a trial-and-error procedure for calculating  $c$ , as described in the next steps, becomes more appropriate.

*Step 5*—Using the value of  $\epsilon_f = \epsilon_{fd}$ , together with an initial assumed value of  $c$ , calculate the concrete strain  $\epsilon_c$  at the top concrete compression fiber from Eq. (10) and calculate the stress in the prestressing steel (Eq. (16)) and the stress in the RS from Eq. (3) and (6) by replacing  $\epsilon_c$  for  $\epsilon_{cu}$ .

*Step 6*—Check equilibrium of forces using Eq. (17) in which  $\epsilon_f = \epsilon_{fd}$ , and  $\alpha_1$  and  $\beta_1$  are as calculated from Eq. (11) and (12).

*Step 7*—Repeat Steps 5 and 6 by revising the neutral axis depth  $c$  until the requirement of force equilibrium in Eq. (17) is satisfied within some degree of tolerance.

*Step 8*—Calculate the nominal moment capacity  $M_n$  at the section under consideration using Eq. (1) in which  $\epsilon_f = \epsilon_{fd}$ .

*Step 9*—Check if  $\phi M_n \geq M_u$ , where  $M_u$  is the load-factored applied moment at the section under consideration obtained by loading the spans (pattern loading) for producing maximum moment at the section under consideration.

The strength-reduction factor  $\phi$  is taken in accordance with the ACI Building Code<sup>1</sup> approach using the relationship between the net tensile strain in the tension reinforcement and the neutral axis depth  $c$  at nominal flexural strength as follows

$$\phi = 0.90 \text{ for } c/d_e \leq 0.38 \quad (20a)$$

$$\phi = 0.65 \text{ for } c/d_e \leq 0.6 \quad (20b)$$

$$\phi = 0.65 + 0.25 \left( 2.73 - 4.55 \frac{c}{d_e} \right) \text{ for } 0.38 \leq c/d_e \leq 0.6 \quad (20c)$$

where  $d_e$  is the equivalent depth of the tension reinforcement (PS, RS, and FRP laminates) expressed as

$$d_e = \frac{(A_{ps} f_{ps} d_p + A_s f_s d + A_f E_f \epsilon_f d_f)}{A_{ps} f_{ps} + A_s f_s + A_f E_f \epsilon_f} \quad (21)$$

## EXPERIMENTAL STUDY

Twenty-four unbonded post-tensioned specimens were tested to evaluate their nominal flexural strength before and after FRP strengthening. An additional six bonded post-tensioned and six RC specimens were also tested for comparison. All 36 specimens were simply supported over a 3.0 m (9.84 ft) span. Dimensions and reinforcement layout are given in Fig. 3. Eighteen of the specimens had a 150 mm (5.9 in.) wide by 250 mm (9.8 in.) deep cross section and a span-depth ratio (depth to center of tension steel) of 15, representing beam members, and the remaining 18 had a 360 mm (14.2 in.) wide by 120 mm (4.7 in.) deep cross section and a span-depth ratio of 35, simulating one-way slab members. The specimen designation, along with areas and depths of reinforcement and other pertinent details and design properties, are summarized in Table 1. The test parameters included, in addition to the span-depth ratio of the member, area of internal prestressed reinforcement for the PC specimens or area of ordinary tension reinforcement for the RC specimens; area of external FRP reinforcement; and tendon profile. Two tendon profiles were selected for each set of specimens: one horizontal and one parabolic.

In the specimens designation provided in Table 1, the first letter U stands for unbonded, B for bonded, and R for reinforced. The second letter B stands for beam, while S stands

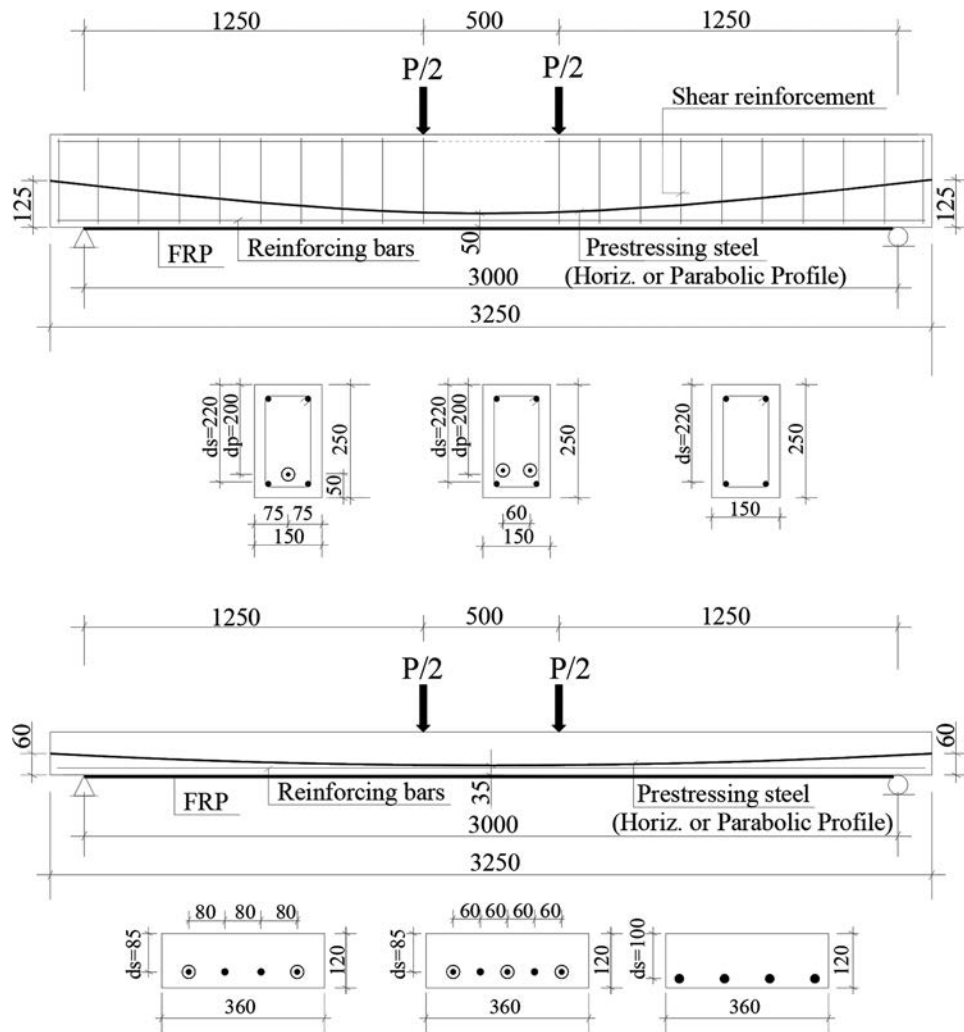


Fig. 3—Typical dimensions and reinforcement details of the beam and slab specimens. (Note: dimensions in mm; 1 mm = 0.039 in.)

for slab. The numbers 1 and 2 following the second letter designate two different levels of PS or RS areas or ratios. Letters H and P designate horizontal and parabolic tendon profile, respectively, and F1 and F2 denote two different levels (areas or layers) of external FRP reinforcement. The parabolic tendon profile in all beam and slab specimens had zero eccentricity at the support.

The prestressing reinforcement consisted of seven-wire strands having 7.9 and 9.5 mm (5/16 and 3/8 in.) diameter, with an area of 37.5 and 52.0 mm<sup>2</sup> (0.058 and 0.08 in.<sup>2</sup>), and actual ultimate strength  $f_{pu}$  of 1958 and 1978 MPa (284 and 287 ksi), respectively. Generated from coupon tests, the actual stress-strain ( $f_{ps} - \epsilon_{ps}$ ) behavior of the two sizes of the prestressing steel were best reproduced using the following relationship<sup>7</sup>

$$f_{ps} = E_{ps} \epsilon_{ps} \left( Q + \frac{1-Q}{\left[ 1 + \left( \frac{E_{ps} \epsilon_{ps}}{K f_{py}} \right)^N \right]^{1/N}} \right) \quad (22)$$

where  $f_{py} = 1670$  MPa (242 ksi),  $E_{ps} = 195,130$  MPa (28,400 ksi),  $N = 14.84$ ,  $K = 1.0$ , and  $Q = 0.0357$  for the 7.9 mm (5/16 in.) strands; and  $f_{py} = 1690$  MPa (245 ksi),  $E_{ps} = 194,440$  MPa (28,200 ksi),  $N = 12.1$ ,  $K = 1.011$ , and  $Q = 0.0301$  for the 9.5 mm (3/8 in.) strands.

All ordinary reinforcing bars (except the 6 mm [0.25 in.] bars) were deformed Grade 60 steel with actual yield strength as given in Table 1. The FRP composite used for strengthening consisted of carbon fiber-reinforced polymer (CFRP) flexible sheets having unidirectional carbon fabric with glass cross-fiber for added strength and fabric stability during installation. The design thickness, the modulus of elasticity, and the ultimate tensile strain of the fibers are 1 mm (0.039 in.), 95,800 MPa (13,895 ksi), and 1%, respectively.

Before casting the specimens, the steel cages were instrumented with electric strain gauges and then placed in plywood formwork ready for concrete casting. The ducts for the post-tensioned steel consisted of galvanized flexible tubes 20 mm (0.79 in.) in diameter. One strand was placed in each duct. For the bonded post-tensioned slab and beam specimens, cement-based grout was injected inside the ducts after the tendons were stressed to provide bond between the strands and concrete. The grout mixture was prepared using Type I portland cement, and proportioned in accordance

**Table 1—Summary of test parameters**

Concrete system	Specimen label	Tendon profile	Prestressing steel			Reinforcing steel					FRP	$f'_c$ , MPa		
			$A_{ps}$	$d_p$ , mm	$f_{se}$ , MPa	$A_s$ , bottom	$d$ , mm	$A_s'$ , top	$A_v$	$f_y$ , MPa	$A_f$ , mm <sup>2</sup> ( $n_f$ )			
Unbonded post-tensioned	Beam	UB1-H	Horizontal	1 (5/16 in.)	200	813	2 (8 mm)	220	—	φ8 at 150	560	—	42	
		UB1-H-F1	Horizontal	1 (5/16 in.)	200	962	2 (8 mm)	220	—	φ8 at 150	612	150 (1)	36	
		UB1-H-F2	Horizontal	1 (5/16 in.)	200	963	2 (8 mm)	220	—	φ8 at 150	612	300 (2)	36	
		UB1-P	Parabolic	1 (5/16 in.)	200	815	2 (8 mm)	220	—	φ8 at 150	560	—	42	
		UB1-P-F1	Parabolic	1 (5/16 in.)	200	971	2 (8 mm)	220	—	φ8 at 150	612	150 (1)	36	
		UB1-P-F2	Parabolic	1 (5/16 in.)	200	781	2 (8 mm)	220	—	φ8 at 150	612	300 (2)	37	
		UB2-H	Horizontal	2 (3/8 in.)	200	778	2 (8 mm)	220	2 (8 mm)	φ8 at 150	560	—	42	
		UB2-H-F1	Horizontal	2 (3/8 in.)	200	924	2 (8 mm)	220	2 (8 mm)	φ8 at 150	612	150 (1)	36	
		UB2-H-F2	Horizontal	2 (3/8 in.)	200	896	2 (8 mm)	220	2 (8 mm)	φ8 at 150	612	300 (2)	37	
		UB2-P	Parabolic	2 (3/8 in.)	200	836	2 (8 mm)	220	2 (8 mm)	φ8 at 150	560	—	42	
		UB2-P-F1	Parabolic	2 (3/8 in.)	200	936	2 (8 mm)	220	2 (8 mm)	φ8 at 150	612	150 (1)	36	
		UB2-P-F2	Parabolic	2 (3/8 in.)	200	923	2 (8 mm)	220	2 (8 mm)	φ8 at 150	612	300 (2)	37	
	Slab	US1-H	Horizontal	2 (5/16 in.)	85	927	2 (8 mm)	92.5	—	—	560	—	42	
		US1-H-F1	Horizontal	2 (5/16 in.)	85	917	2 (8 mm)	92.5	—	—	612	150 (1)	36	
		US1-H-F2	Horizontal	2 (5/16 in.)	85	964	2 (8 mm)	92.5	—	—	612	300 (1)	36	
		US1-P	Parabolic	2 (5/16 in.)	85	886	2 (8 mm)	98.5	—	—	560	—	42	
		US1-P-F1	Parabolic	2 (5/16 in.)	85	949	2 (8 mm)	98.5	—	—	612	150 (1)	36	
		US1-P-F2	Parabolic	2 (5/16 in.)	85	971	2 (8 mm)	98.5	—	—	612	300 (1)	37	
		US2-H	Horizontal	3 (3/8 in.)	85	804	2 (8 mm)	92.5	—	—	560	—	42	
		US2-H-F1	Horizontal	3 (3/8 in.)	85	912	2 (8 mm)	92.5	—	—	612	150 (1)	36	
		US2-H-F2	Horizontal	3 (3/8 in.)	85	858	2 (8 mm)	92.5	—	—	612	300 (1)	37	
		US2-P	Parabolic	3 (3/8 in.)	85	831	2 (8 mm)	98.5	—	—	560	—	42	
		US2-P-F1	Parabolic	3 (3/8 in.)	85	921	2 (8 mm)	98.5	—	—	612	150 (1)	36	
		US2-P-F2	Parabolic	3 (3/8 in.)	85	916	2 (8 mm)	98.5	—	—	612	300 (1)	37	
Bonded post-tensioned	Beam	BB2-P	Parabolic	2 (3/8 in.)	200	884	2 (6 mm)	220	2 (6 mm)	φ8 at 150	0	—	37	
		BB2-P-F1	Parabolic	2 (3/8 in.)	200	894	2 (6 mm)	220	2 (6 mm)	φ8 at 150	0	150 (1)	37	
		BB2-P-F2	Parabolic	2 (3/8 in.)	200	885	2 (6 mm)	220	2 (6 mm)	φ8 at 150	0	300 (2)	37	
	Slab	BS2-P	Parabolic	3 (3/8 in.)	85	970	2 (8 mm)	98.5	—	—	0	—	37	
		BS2-P-F1	Parabolic	3 (3/8 in.)	85	915	2 (8 mm)	98.5	—	—	0	150 (1)	37	
		BS2-P-F2	Parabolic	3 (3/8 in.)	85	892	2 (8 mm)	98.5	—	—	0	300 (1)	37	
Reinforced concrete	Beam	RB2	—	—	—	—	2 (16 mm)	220	—	φ8 at 100	530	—	37	
		RB2-F1	—	—	—	—	2 (16 mm)	220	—	φ8 at 100	530	150 (1)	37	
		RB2-F2	—	—	—	—	2 (16 mm)	220	—	φ8 at 100	674	300 (2)	37	
	Slab	RS2	—	—	—	—	—	4 (12 mm)	100	—	—	555	—	37
		RS2-F1	—	—	—	—	—	4 (12 mm)	100	—	—	555	150 (1)	37
		RS2-F2	—	—	—	—	—	4 (12 mm)	100	—	—	624	300 (1)	37

Note: 1 in. = 25.4 mm; 1 MPa = 0.145 ksi; 1 mm<sup>2</sup> = 0.0016 in.<sup>2</sup>.

with the ACI Building Code<sup>1</sup> with a water-cement ratio of 0.40.

The CFRP sheets were attached to the bottom tension face of the beam and slab specimens in accordance with

the manufacturer's recommendations and in compliance with the ACI Committee 440<sup>2</sup> recommendation for securing proper development length. No particular measures were taken to improve bond strength between the FRP and the

substrate. One or two layers of 150 mm (5.9 in.) wide FRP sheets were applied for the beam specimens, while only one layer of 150 or 300 mm (5.9 or 11.8 in.) wide sheets was applied for the slab specimens (Table 1).

All specimens were tested in four-point bending using two symmetrical concentrated loads spaced a distance equal to 1/6 the span length, or 500 mm (19.7 in.) apart (Fig. 3). It should be noted that because the increase in tendon strain/stress (above effective prestrain/prestress) of unbonded members due to increase in applied load depends on the overall deformation of the member or elongation of the tendon between the anchorages, the ultimate tendon stress and flexural capacity of unbonded members are influenced by the geometry of applied load.<sup>8</sup> Two-point loads spaced at 1/6 the span length were found analytically<sup>8,9</sup> to be equivalent to uniform load application for predicting the ultimate tendon stress and moment capacity of unbonded post-tensioned members.

To replicate actual conditions of concrete flexural members that require strengthening or repair, all control and strengthened specimens were first subjected to cyclic loading consisting of six cycles before the FRP application, and another six cycles after FRP application, ranging between a minimum load  $P_{min}$  and a maximum load  $P_{max}$ , simulating dead load and dead plus live load, respectively. The loads  $P_{min}$  and  $P_{max}$  were set at 30 and 70%, respectively, of the calculated nominal load capacity of the specimens.

For the control or unstrengthened specimens, the cyclic loading stage was followed immediately by a stage of monotonically increasing load until complete flexural failure of the specimens. The specimens that were strengthened using CFRP were first subjected to the same cyclic loading protocol as the control specimens, and then unloaded to prepare them for CFRP application. Following at least 7 days of CFRP application, the strengthened specimens were subjected to a loading protocol consisting of cyclic loading and monotonically increasing load to failure, similar to the control specimens.

Test measurements included strains and stresses in the prestressing strands, CFRP laminates, and reinforcing bars of the RC specimens within the constant moment region close to midspan; applied load; and deflection. Crack patterns were also monitored throughout the test for each specimen. The strains were measured using electric strain gauges, while deflection was measured using a linear voltage differential transformer (LVDT). The test results were automatically collected and recorded using a data acquisition and control system.

#### DISCUSSION OF RELEVANT TEST RESULTS

Typical photos of the specimens at the conclusion of the test are shown in Fig. 4. Representative modes of failure and cracking patterns at nominal strength for the unbonded PC beam specimens in comparison with the bonded PC and RC beam specimens are provided in Fig. 5. Flexural failure for the various beam and slab specimens occurred either by concrete crushing or by FRP debonding or fracturing. Relevant experimental results at nominal flexural strength including load capacity, deflection, stress in the prestressing

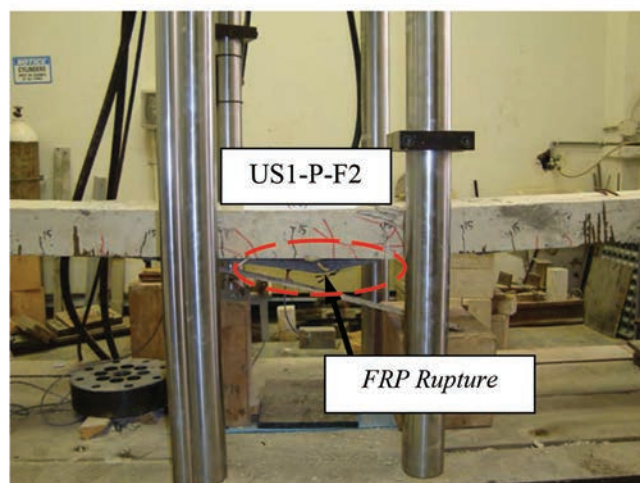
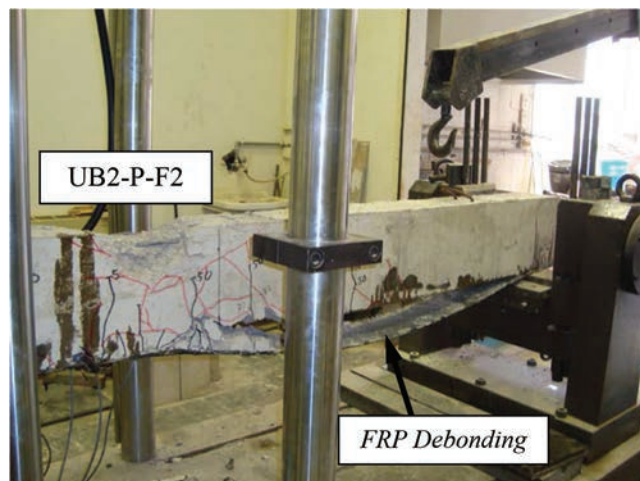


Fig. 4—Typical photos of specimens at conclusion of test.

steel, strain in the CFRP reinforcement, and mode of failure are all summarized in Table 2. Representative variations of deflection, FRP strain, and stress increase in the prestressing steel above effective prestress  $f_{se}$  with applied load are shown in Fig. (6) through (9), respectively.

The crack patterns for the unbonded beam specimens (Fig. 5) and the slab specimens (not shown for brevity) were similar to those developed in the companion bonded specimens. The spreading of cracks outside the constant moment region increased with the use of FRP reinforcement and as the area of FRP reinforcement increased, and was most significant for the RC specimens (Fig. 5).

It is clear from the test data summarized in Table 2 that the use of FRP reinforcement significantly increased the moment capacity of unbonded post-tensioned members. The corresponding increase grew higher as the area of FRP reinforcement increased, and varied between 24 and 105% for the beam specimens and between 21 and 126% for the slab specimens of the current investigation. As would be expected, however, the increases in load capacities were accompanied with reductions in ductility or ultimate deformation capacities, which were most notable for the beam specimens. The reductions in deformation capacity, which are attributed in

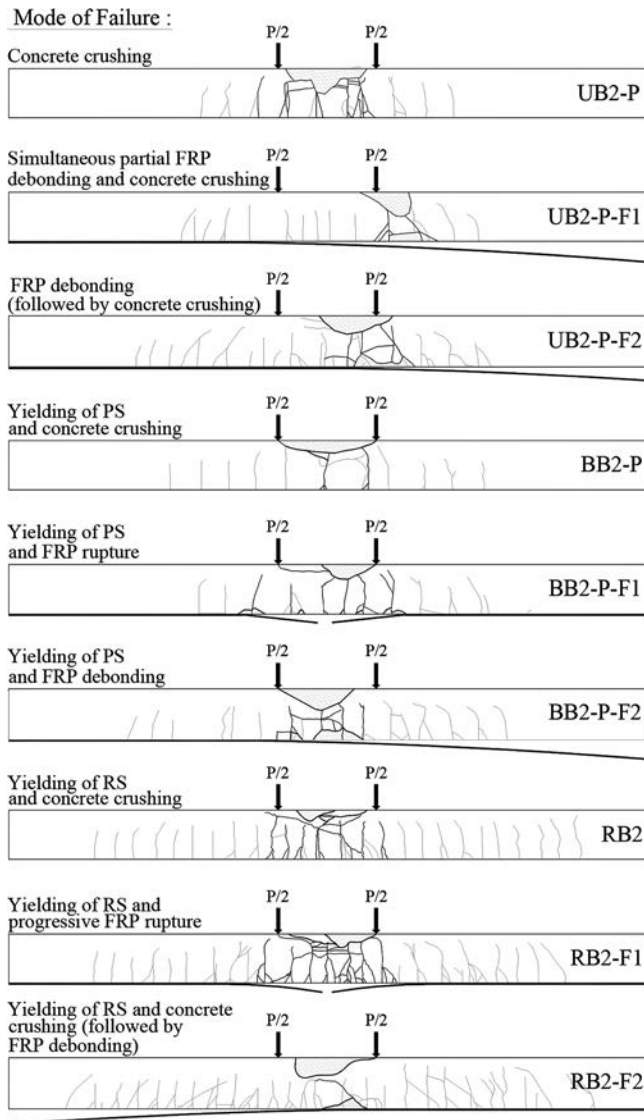


Fig. 5—Typical comparison of crack pattern for unbonded PC, bonded PC, and RC beam specimens.

part to the FRP debonding mode of flexural failure, were almost identical for the slab or beam specimens reinforced with Level F1 and F2 FRP reinforcement (Table 2).

The FRP strain/stress developed at flexural failure (Fig. 8 and Table 2) generally decreased as the area of FRP reinforcement increased within the specimens of the same test series, or as the area of prestressing reinforcement increased. The overall average FRP strains at ultimate for the combined beam and slab specimens strengthened using the two different areas or levels (F1 and F2) of FRP reinforcement were 6260 to 5400  $\mu\epsilon$  for the unbonded PC, 6875 to 4970  $\mu\epsilon$  for the bonded PC, and 7608 to 5419  $\mu\epsilon$  for the RC specimens, respectively.

Being unbonded, the stress in the prestressing steel at nominal flexural strength was below yield for all specimens. The corresponding strain (Table 2) decreased as the area of FRP reinforcement increased. On the other hand, the strains and stresses in the prestressing steel for all companion bonded PC beam and slab specimens exceeded yield and

were significantly larger than the stresses developed in the unbonded specimens.

Based on the experimental results and observations of the current investigation, it was obvious that the cracking and crack patterns, increase in load capacities, reduction in deformation capacities, and modes of flexural failure of the unbonded PC specimens as a result of FRP strengthening were quite similar to those of the bonded PC and RC specimens. More test data and a detailed discussion of test results are reported elsewhere.<sup>10</sup>

## COMPARISON OF ANALYTICAL PREDICTIONS WITH TEST DATA

Table 2 shows comparisons of the predictions of the proposed design-oriented approach developed in this study for FRP-strengthened unbonded PC members together with the predictions of the ACI Committee 440<sup>2</sup> approach for bonded PC and RC members against the test results generated in the experimental part of this investigation. These include stress  $f_{ps}$  in the prestressing steel, strain  $\epsilon_f$  in the FRP reinforcement, mode of flexural failure, and nominal moment capacity  $M_n$ . In calculating the stress in the prestressing steel and the nominal moment capacity, the reduction factors  $\phi_{ps}$  and  $\psi_f$  were both set equal to 1.0. Also, because the load at which the FRP was applied was very small (equal to the self-weight of the specimen), the initial substrate strain  $\epsilon_{bi}$  was taken equal to zero.

Figure 10 shows predicted stress increase  $\Delta f_{ps}$  ( $\Delta f_{ps} = f_{ps} - f_{se}$ ) and total stress  $f_{ps}$  in the prestressing steel at ultimate versus test results for the unbonded prestressed beams and slab specimens of the current investigation. The data are superimposed on predicted versus test results of a collection of unbonded members (without FRP reinforcement) compiled and reported previously.<sup>5,6</sup> The compiled data correspond to internally or externally post-tensioned simply supported members, and continuous members having two or three spans, and loaded with two-point or single-point loads, respectively. Figure 11 shows predicted versus measured nominal moment capacities for the 36 beam and slab specimens tested in this investigation.

Given the inevitable scatter associated with the prediction of the stress in unbonded tendons at ultimate, it can be seen from Fig. 10 that the proposed analytical approach predicted the test data with reasonable accuracy. More conservative predictions can be obtained by using the stress reduction parameter  $\phi_{ps} = 0.7$  proposed for design purposes. As expected, the stress predictions for the bonded members were more accurate than the unbonded members. The average ratio of the test-to-predicted tendon stress were 1.10 (standard deviation [SD] = 0.12) for the unbonded specimens, and 1.02 (SD = 0.04) for the bonded specimens. It should be noted that due to the presence of 2 $\phi$ 8 mm ordinary steel bars, which are required as minimum bonded reinforcement in accordance with the ACI Building Code,<sup>1</sup> the control unbonded PC specimens developed well-distributed cracks along their length as opposed to the development of few cracks or concentration of deformation at a single crack that normally occurs in members with an unbonded tendon system.<sup>5</sup> In other words, the equivalent plastic hinge length

**Table 2—Summary of test results and analytic predictions**

Specimen	$P_u$ (kN)	$\Delta_u$ (mm)	$f_{ps}$ (MPa)			FRP Strain $\epsilon_f$			Mode of failure		Nominal moment $M_u$ (kN-m)		
	Exp.	Exp.	Exp.	Analysis	Exp./ Analysis	Exp.	Analysis	Exp./ Analysis	Experiment	Analysis	Exp.	Analysis	Exp./ Analysis
UB1-H	42.3	64	1567	1253	1.25	—	—	—	Concrete crushing	Concrete crushing	26.4	20.8	1.27
UB1-H-F1	66.9	31	1303	1250	1.04	7122	7948*	0.90	FRP debonding	FRP debonding	41.8	46.5	0.90
UB1-H-F2	86.9	33	1223	1290	0.95	5378	5620*	0.96	FRP debonding	FRP debonding	54.3	55.6	0.98
UB1-P	46.8	81	1669	1255	1.33	—	—	—	Concrete crushing	Concrete crushing	29.3	20.8	1.41
UB1-P-F1	66.3	35	1413	1259	1.12	4556	7948*	0.57	FRP debonding	FRP debonding	41.4	46.5	0.89
UB1-P-F2	89.0	36	1102	1098	1.00	5604	5698*	0.98	FRP debonding	FRP debonding	55.6	55.2	1.01
UB2-H	63.6	43	1246	1205	1.03	—	—	—	Concrete crushing	Concrete crushing	39.8	35.3	1.13
UB2-H-F1	80.8	26	1163	1230	0.95	6934	7949*	0.87	Partial rupture + partial debonding	FRP debonding	50.5	60.4	0.84
UB2-H-F2	104.8	31	1122	1239	0.91	5329	5698*	0.94	FRP debonding	FRP debonding	65.5	68.9	0.95
UB2-P	75.2	88	1598	1260	1.27	—	—	—	Concrete crushing	Concrete crushing	47.0	36.3	1.29
UB2-P-F1	93.6	37	1339	1244	1.08	5393	7948*	0.68	FRP debonding + concrete crushing	FRP debonding	58.5	60.6	0.97
UB2-P-F2	101.2	30	1223	1270	0.96	4285	5698*	0.75	FRP debonding	FRP debonding	63.3	69.3	0.91
US1-H	22.7	62	1211	1106	1.09	—	—	—	Concrete crushing	Concrete crushing	14.2	11.5	1.23
US1-H-F1	34.3	63	1195	1033	1.16	8309	7948*	1.05	FRP rupture	FRP debonding	21.4	23.3	0.92
US1-H-F2	43.0	66	1152	1112	1.04	6074	6490	0.94	Partial rupture + partial debonding	Concrete crushing	26.9	30.1	0.89
US1-P	21.3	100	1413	1066	1.33	—	—	—	Concrete crushing	Concrete crushing	13.3	11.6	1.15
US1-P-F1	34.5	68	1177	1065	1.11	5770	7948*	0.73	FRP debonding	FRP debonding	21.6	23.8	0.91
US1-P-F2	48.1	75	1165	1117	1.04	6280	6580	0.95	FRP rupture + concrete crushing	Concrete crushing	30.1	30.8	0.97
US2-H	35.1	87	1227	966	1.27	—	—	—	Concrete crushing	Concrete crushing	21.9	16.3	1.34
US2-H-F1	42.6	62	—	1039	—	6277	6758	0.93	Concrete crushing + partial debonding	Concrete crushing	26.6	26.4	1.01
US2-H-F2	57.2	75	1065	972	1.10	5517	5551	0.99	Concrete crushing	Concrete crushing	35.8	31.6	1.13
US2-P	36.9	66	1105	992	1.11	—	—	—	Concrete crushing	Concrete crushing	23.1	17.0	1.36
US2-P-F1	47.6	68	1146	1047	1.09	7554	6731	1.12	Concrete crushing	Concrete crushing	29.8	26.9	1.11
US2-P-F2	59.8	67	1136	1029	1.10	5570	5429	1.03	Concrete crushing	Concrete crushing	37.4	32.1	1.16
BB2-P	63.4	44	1738	1737	1.00	—	—	—	Concrete crushing	Concrete crushing	39.6	34.2	1.16
BB2-P-F1	87.0	35	1710	1682	1.02	5906	7027	0.84	FRP rupture	Concrete crushing	54.4	53.6	1.01
BB2-P-F2	107.8	30	1680	1591	1.06	4781	5523*	0.87	FRP debonding	FRP debonding	67.4	63.1	1.07
BS2-P	33.9	71	1662	1687	0.99	—	—	—	Concrete crushing	Concrete crushing	21.2	21.4	0.99
BS2-P-F1	44.3	67	1702	1556	1.09	7834	6000	1.31	FRP debond. and rupture	Concrete crushing	27.7	28.1	0.98
BS2-P-F2	59.7	70	1429	1435	1.00	5701	5045	1.13	Concrete crushing	Concrete crushing	37.3	32.2	1.16
RB2	72.5	46	—	—	—	—	—	—	Concrete crushing	Concrete crushing	45.3	42.5	1.07
RB2-F1	98.6	35	—	—	—	7608	6740	1.13	FRP rupture	Concrete crushing	61.6	62.0	0.99
RB2-F2	110.8	33	—	—	—	5003	4177	1.20	Concrete crushing	Concrete crushing	69.3	73.4	0.94
RS2	37.0	77	—	—	—	—	—	—	Concrete crushing	Concrete crushing	23.1	22.7	1.02
RS2-F1	48.5	60	—	—	—	—	6863	—	FRP rupture	Concrete crushing	30.3	32.2	0.94
RS2-F2	66.7	77	—	—	—	5834	4660	1.25	FRP rupture	Concrete crushing	41.7	36.6	1.14

\*Equal to debonding strain calculated using Eq. (8).

Notes: Exp. is Experiment; 1 kN = 0.224 kip; 1 mm = 0.039 in.; 1 MPa = 0.145 ksi; 1 kN-m = 8.83 k-in.)



Fig. 6—Comparison between load-deflection response of unbonded and bonded PC beam specimens. (Note: 1 mm = 0.039 in.; 1 kN = 0.224 kip.)

developed in these specimens was, admittedly, larger than that predicted from  $l_p = (20.7/f + 10.5)c$ , based on which Eq. (13) and (16) were developed. Consequently, the ultimate strains or stresses in the prestressing steel for the control specimens in this investigation (Table 2 and Fig. 10) were conservatively larger than those predicted by Eq. (13) or (16).

Also, as can be seen from Table 2, the analytical approach predicted the experimentally measured strain in the FRP reinforcement and associated mode of flexural failure reasonably accurately for most unbonded specimens, as well as for the bonded PC and RC specimens. While the results are, to a great extent, in support of the ACI Committee 440<sup>2</sup> guidelines for predicting modes of flexural failure in FRP-strengthened members, the experimentally measured FRP strains for the unbonded specimens were consistently slightly lower than those predicted using Eq. (8). The average ratio of test-to-predicted FRP strains is calculated at 0.9 (SD = 0.15) for the unbonded specimens, 1.1 (SD = 0.18) for the combined bonded PC and RC specimens, and 0.96 (SD = 0.18) for all unbonded, bonded, and RC specimens.

Finally, from Fig. 11, Table 2, and the statistical data provided, except for the control unbonded PC specimens that developed larger than predicted moment capacities due to the development of larger-than-predicted steel stresses,

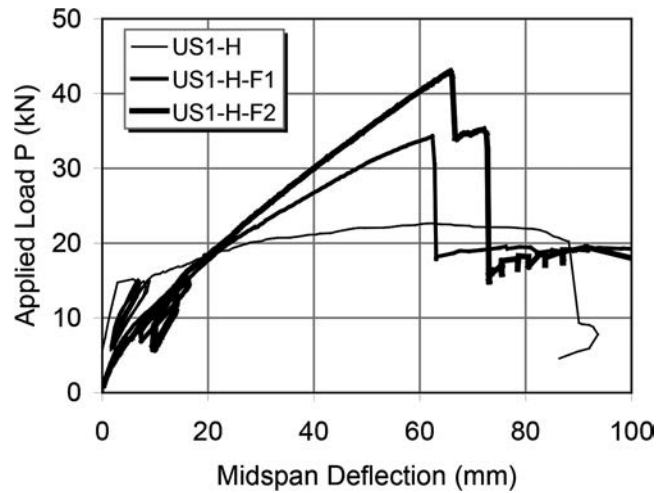


Fig. 7—Representative load-deflection response of slab specimens. (Note: 1 mm = 0.039 in.; 1 kN = 0.224 kip.)

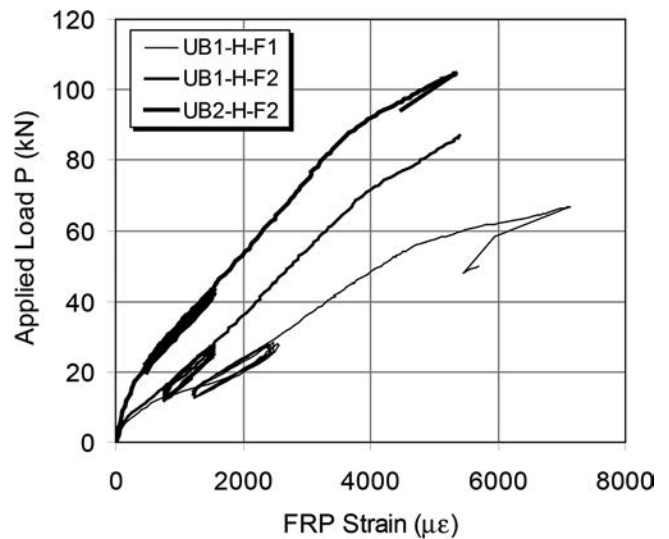


Fig. 8—Representative variation of FRP strain with applied load. (Note: 1 kN = 0.224 kip.)

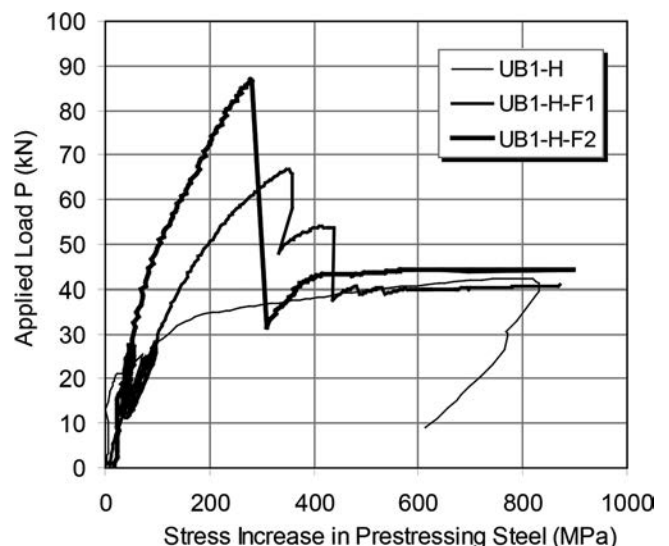


Fig. 9—Typical variation of stress increase in unbonded prestressing steel with applied load. (Note: 1 kN = 0.224 kip.)

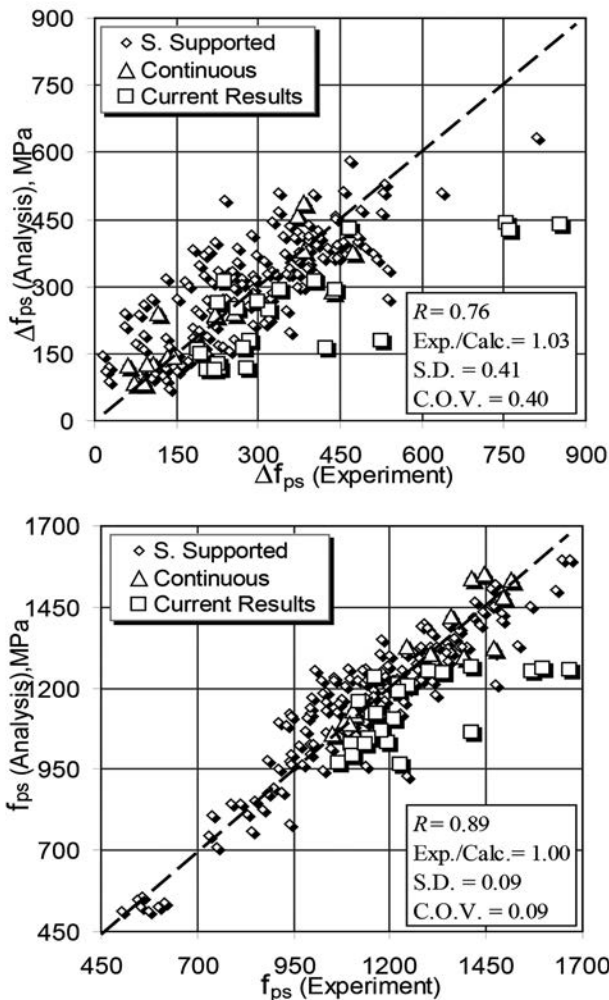


Fig. 10—Prediction of experimental data for unbonded members<sup>6</sup> including FRP strengthened unbonded specimens of current investigation for  $\phi_{ps} = 1.0$ . (Note: 1 MPa = 0.145 ksi.)

as illustrated previously, the predicted nominal moment capacities  $M_n$  of the FRP-strengthened specimens (assuming  $\psi_f = 1.0$ ) were generally in good agreement with the test results. Despite little discrepancy, the level of accuracy in predicting  $M_n$  for the unbonded specimens using the proposed design approach is consistent with the level of accuracy in predicting  $M_n$  for bonded PC and RC specimens using the ACI Committee 440<sup>2</sup> approach. The average ratio of test-to-predicted results is calculated as 0.97 (SD = 0.09) for the FRP-strengthened unbonded specimens, and 1.05 (SD = 0.09) for the combined FRP-strengthened bonded PC and RC specimens. For the combined control and FRP-strengthened specimens, the coefficient of correlation  $R$  between the experimentally measured and the calculated nominal moment capacities is equal to 0.97 for the unbonded specimens, 0.98 for the bonded PC and RC specimens, and 0.97 for the overall unbonded PC, bonded PC, and RC specimens. Their corresponding average ratios of test-to-predicted results are equal to 1.07 (SD = 0.17), 1.04 (SD = 0.08), and 1.06 (SD = 0.15).

It should be noted that because the experimentally measured FRP strains of the FRP-strengthened unbonded

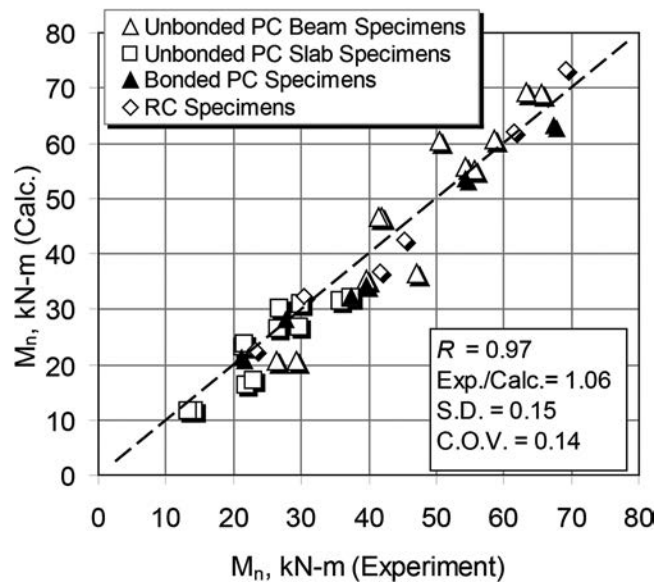


Fig. 11—Prediction of nominal moment capacity of combined specimens of current investigation. (Note: 1 kN-m = 8.83 k-in.)

specimens, particularly when the mode of failure is by FRP debonding or rupture, were slightly lower than those predicted by Eq. (8), these specimens developed slightly lower moment capacities than those predicted using the proposed approach (Table 2). Consequently, although additional conservatism in predicting  $M_n$  for design purposes can be gained by setting  $\psi_f = 0.85$  as recommended by ACI Committee 440<sup>2</sup> (Eq. (1)), the FRP debonding strain in Eq. (8) may require slight modification in its application for unbonded members. Until further experimental evidence is available to support such modification, however, Eq. (8) can still be used for unbonded members without significant loss of accuracy.

## CONCLUSIONS

A design-oriented approach for calculating the nominal moment capacity  $M_n$  of unbonded PC members when strengthened using external FRP composites is presented. The approach is applicable for simply supported and continuous members, and is consistent with the guidelines of ACI Committee 440<sup>2</sup> for evaluating  $M_n$  of bonded PC or RC members. The accuracy of the proposed approach for simply supported members was verified by comparing with the results of a comprehensive test program designed and carried out specifically for the purpose of this study.

Except for a slight discrepancy in predicting the FRP debonding strain for the unbonded specimens that encountered FRP failure before concrete crushing, the proposed approach for unbonded PC members, and the approach recommended by ACI Committee 440 for bonded PC and RC members, predicted well the test results at ultimate, including the strain/stress in the PS, strain in the FRP reinforcement, mode of flexural failure, and nominal flexural strength.

The experimental results and the proposed approach for calculating  $M_n$  of FRP-strengthened unbonded PC members clearly show that the use of external FRP reinforcement is as effective in improving the nominal flexural strength of

unbonded PC members, as when used for strengthening bonded PC or RC members. Consequently, in designing the FRP system for flexural strengthening of unbonded PC members, no special guidelines are needed beyond those recommended in the ACI Committee 440<sup>2</sup> report and the design-oriented approach proposed for unbonded members in this investigation.

### AUTHOR BIOS

**Fatima El Meski** is a Lecturer at the Lebanese American University, Beirut, Lebanon. She was formerly a PhD Student in the Department of Civil and Environmental Engineering at the American University of Beirut, Beirut, Lebanon.

ACI member **Mohamed H. Harajli** is a Professor of civil engineering at the American University of Beirut. His research interests include design and behavior of reinforced, prestressed, and fiber-reinforced concrete members and strengthening and repair of concrete structures.

### REFERENCES

1. ACI Committee 318, "Building Code Requirements for Reinforced Concrete and Commentary (ACI 318-11)," American Concrete Institute, Farmington Hills, MI, 2011, 503 pp.
2. ACI Committee 440, "Guide for the Design and Construction of Externally Bonded FRP Systems for Strengthening Concrete Structures (ACI

440.2R-08)," American Concrete Institute, Farmington Hills, MI, 2008, 76 pp.

3. AASHTO, "LRFD Bridge Design Specifications," American Association of State Highway and Transportation Officials, Washington, DC, 2004, 1324 pp.

4. Naaman, A. E.; Burns, N.; French, C.; Gamble, W. L.; and Mattock, A. H., "Stresses in Unbonded Prestressing Tendons at Ultimate: Recommendation," *ACI Structural Journal*, V. 99, No. 4, July-Aug. 2002, pp. 518-529.

5. Harajli, M. H., "On the Stress in Unbonded Tendons at Ultimate: Critical Assessment and Proposed Changes," *ACI Structural Journal*, V. 103, No. 6, Nov.-Dec. 2006, pp. 803-812.

6. Harajli, M. H., "Tendon Stress at Ultimate in Continuous Unbonded Post-Tensioned Members: Proposed Modification of ACI Eq. (18-4) and (18-5)," *ACI Structural Journal*, V. 109, No. 2, Mar.-Apr. 2012, pp. 183-192.

7. Menegotto, M., and Pinto, P. E., "Method of Analysis for Cyclically Loaded Reinforced Concrete Plane Frames." *IABSE Preliminary Report for Symposium on Resistance and Ultimate Deformability of Structures Acted on Well-Defined Repeated Loads*, Lisbon, Portugal, 1973, pp. 15-22.

8. Harajli, M. H., and Hijazi, S., "Evaluation of the Ultimate Steel Stress in Unbonded Partially Prestressed Beams," *PCI Journal*, V. 36, No. 2, Jan.-Feb. 1991, pp. 62-82.

9. Moon, J. H., and Burns, N. H., "Flexural Behavior of Members with Unbonded Tendons. II: Application," *Journal of Structural Engineering*, ASCE, V. 123, No. 8, Aug. 1997, pp. 1095-1101.

10. El Meski, F., "Behavior of Unbonded Post Tensioned Members Strengthened Using External FRP Composites: Experimental Evaluation and Analytic Modeling," PhD dissertation, Department of Civil and Environmental Engineering, American University of Beirut, Beirut, Lebanon, 2012, 283 pp.